Proceedings of the ASME 2010 3rd Joint US-European Fluids Engineering Summer Meeting and 8th International Conference on Nanochannels, Microchannels, and Minichannels
FEDSM-ICNMM2010
August 1-5, 2010, Montreal, Canada

FEDSM-ICNMM2010-30392

CFD BASE HYDRO-TURBINE OPTIMIZATION – SIMULATION OF FLOW OVER A ROTATING BLADE USING IMMERSED-BOUNDARY METHOD

Ning Zhang (Ph.D.)
Department of Engineering
McNeese State University
Lake Charles, Louisiana, USA

Saikiran Yadagiri
Department of Engineering
McNeese State University
Lake Charles, Louisiana, USA

Brent Ballard
Gulfstream Technologies
Olney, Texas, USA

Reggy Saxon
ReCon Engineering Inc.
Lake Charles, Louisiana, USA

Willi Schippers (P.E.)
ReCon Engineering Inc.
Lake Charles, Louisiana, USA

ABSTRACT

The shape of the hydro-turbine blade has significant effects on turbine efficiency. In this paper, CFD base shape optimization was performed to assist in the design of Gulfstream Technologies GreenFlow Turbines™. A novel immersed-boundary method (1) was used to simulate flow over a rotating blade. The method was validated previously using literature data and was proven to be accurate and efficient for simulation of flow over moving objects. Several different blade shapes were tested, as well as the pivot locations of the blade. The complex flow characteristics were revealed from the simulation results. The time-histories of force distributions on the surfaces of the blades were recorded and analyzed to determine the optimal shape and pivot location which would result in generating the most power output.

INTRODUCTION

The turbine blade in this study is an airfoil shaped blade. The motion of the blade is rotating around a pivot point on the blade. There are many previous investigations of flow over flapping airfoil which mimics the flying motion of bird and insects. Experimentally, a thorough review of experimental work in flapping biomimetic foils was provided by Triantafyllou et al. (2). Jone et al. (3) performed experiments for heaving only airfoil, while Koochesfahani (4) did for pitching only airfoil. For heaving and pitching combined motion, several researchers performed the experiments (5-8). Numerically, this problem was not studied significantly until recently due to the development of the immersed-boundary method (IBM). The numerical studies include Lu et al. (9), Dong et al. (10) and Webb et al. (8). However, previous numerical studies of flow over a rotating airfoil are scarce, due to the difficulties in simulating moving objects. Shen and Sorensen (11) performed modeling for a rotating airfoil in which the rotating blade was approximated using an order of magnitude analysis on spanwise derivatives. In the present study, a direct numerical simulation was performed for flow over a rotating airfoil using the IBM.

The IBM for fluid-structure interaction problems typically discretize the equations of motion for the fluid on a Cartesian grid, because such methods generally do not require that the geometry of the structure conform in any way to the Cartesian grid. The early development of IBM includes the feedback forcing method (12,13) and direct forcing method (14). Recently, more complicated immersed-boundary (IB) treatments have been developed that include Fadlun et al. (15), Ravoux et al. (16), Tseng and Ferziger (17) and Mittal and Iaccarino (18). The advantages of the present IBM used in this paper (1) include: a smooth representation of IB surface; improve accuracy near the boundary without higher-order or more complicated schemes; easy implementation; no Reynolds

number restriction; no stability problem; and low computational cost.

NUMERICAL METHOD

In the present immersed-boundary method, the nondimensional equations for incompressible fluid flow are

$$\frac{\partial \mathbf{u}}{\partial t} + \mathbf{u}\cdot\nabla\mathbf{u} = -\nabla P + \frac{1}{\mathbf{Re}}\nabla^2\mathbf{u} + \mathbf{f} \tag{1}$$

and

$$\nabla\mathbf{u} = 0, \tag{2}$$

where **f** is the body force representing the boundary force. The forcing term **f**, which functions as a velocity corrector for the grid points immediately inside the immersed boundary, is prescribed at each time step to establish the desired boundary moving velocity. For a time-marching scheme, this force can be expressed as

$$\mathrm{f} = \frac{1}{N}\sum_{n=1}^{N} D_n\{\frac{1}{\Delta t}[\mathbf{v}-\mathbf{u}(\mathbf{x}_s)] + \mathbf{u}\cdot\nabla\mathbf{u} + \nabla P - \frac{1}{\mathbf{Re}}\nabla^2\mathbf{u}\}\cdot \tag{3}$$

In the above equation, D_n is the weighting function, N is the number of IB points affecting it, and v is the physical boundary velocity and $\mathbf{u}(x_s)$ is the computed boundary velocity. The magnitude of this force in Eq. (3) is determined by the bilinear weighting function which continuously changes from 1 to 0. Therefore, the force itself is continuously distributed in the computational domain. Note that if the current grid point coincides with an IB point, D_n is 1 and the velocity on the grid point can be fully corrected to the physical velocity on the surface, **v**.

RESULTS AND DISCUSSIONS

The present IBM was validated using the cases of flow over a stationary or oscillating cylinder (1, 19), flow over a flapping airfoil (20). The method has also been used to simulate flow over single and tandem swimming fish, in which the fish was represented by an airfoil in wavy motion (21).

In the present flow over a counter-clockwise rotating turbine blade simulation, the NACA0012 airfoil was used as the original blade shape. The thickness then was increased by 1.333 time, and 1.667 times to investigate the blade thickness effect. The original pivot was at 1/3 of the chord length from the leading edge, and was then changed to 1/2 and 2/3 to study the effect from the pivot location. The Reynolds number was set as 1000 for all the cases. The dimensionless time for one rotation cycle is 18 based on the actual operating condition of the hydro turbine. The surface pressure coefficient, C_p, was the primary parameter to be investigated. The flow structures around and downstream of the rotating blade was also revealed.

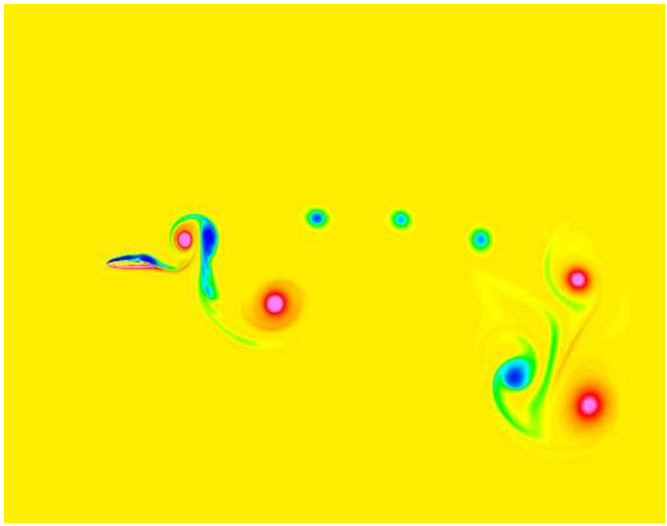

(a) original blade, 1/3 pivot

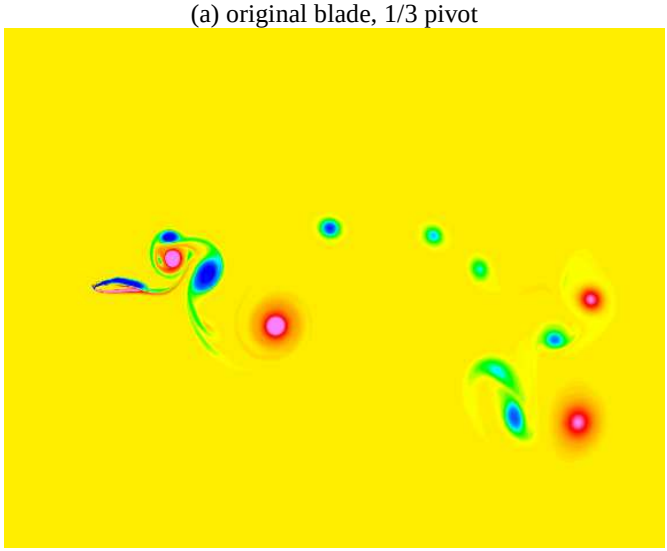

(b) original blade, 2/3 pivot

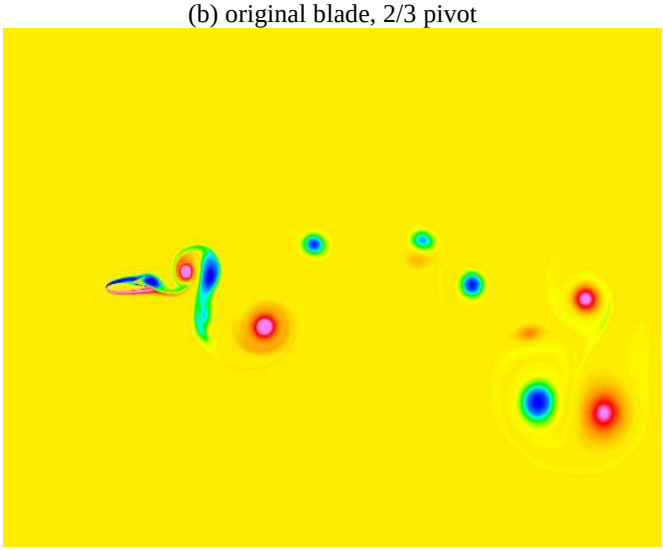

(c) thickest blade, 1/3 pivot

Figure 1, vorticity contours at the initial position

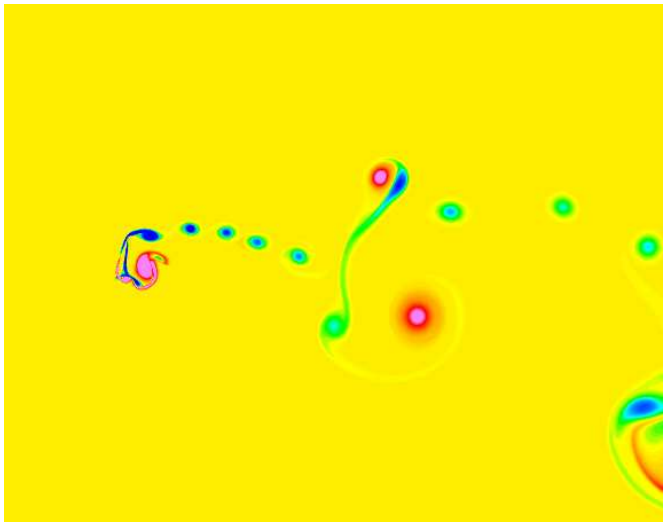

(a) original blade, 1/3 pivot

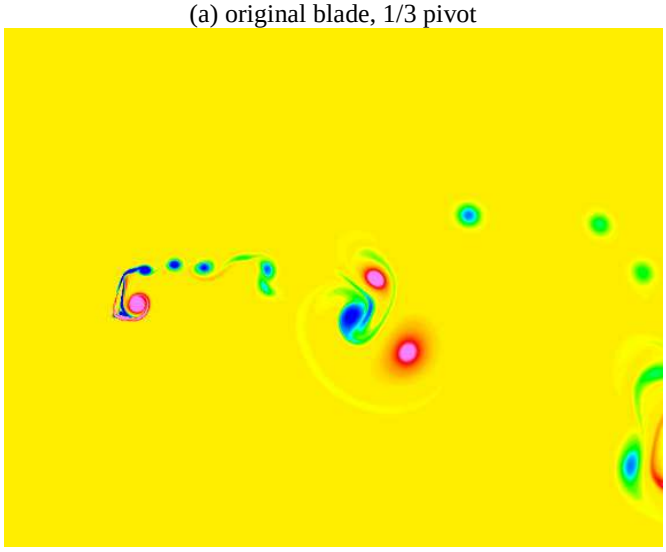

(b) original blade, 2/3 pivot

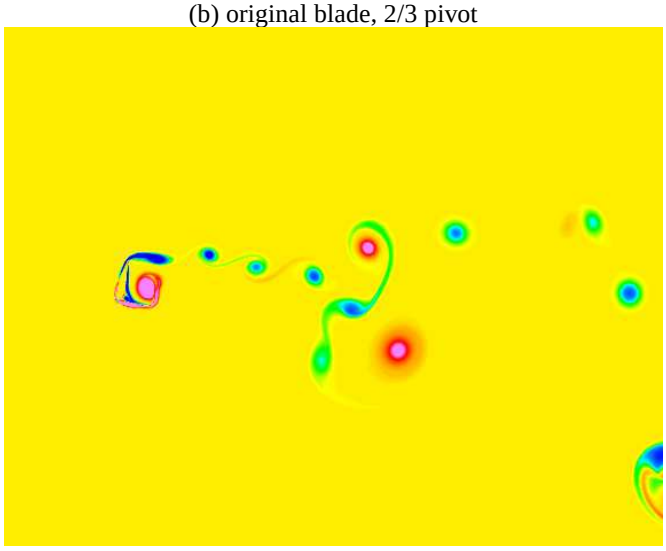

(c) thickest blade, 1/3 pivot

Figure 2, vorticity contours at blade position after 1/4 rotation

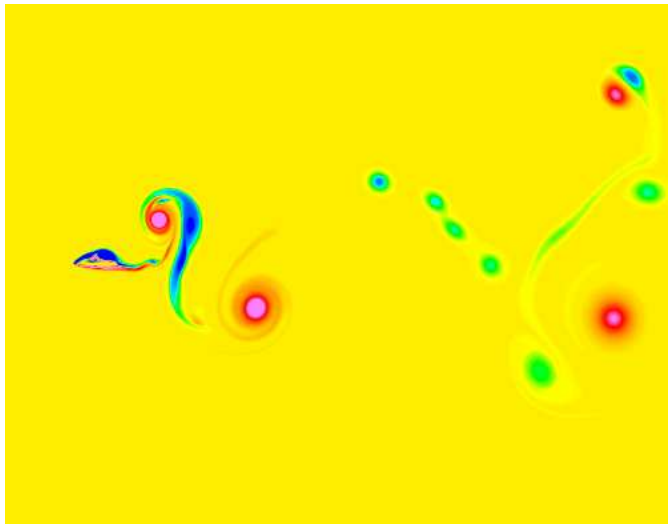

(a) original blade, 1/3 pivot

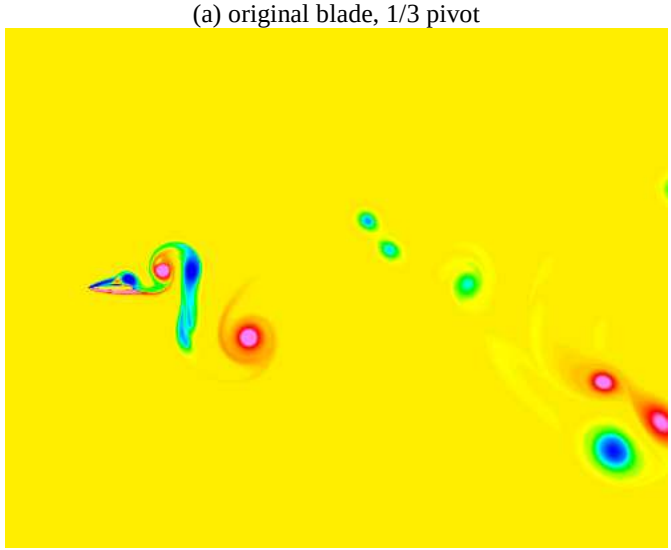

(b) original blade, 2/3 pivot

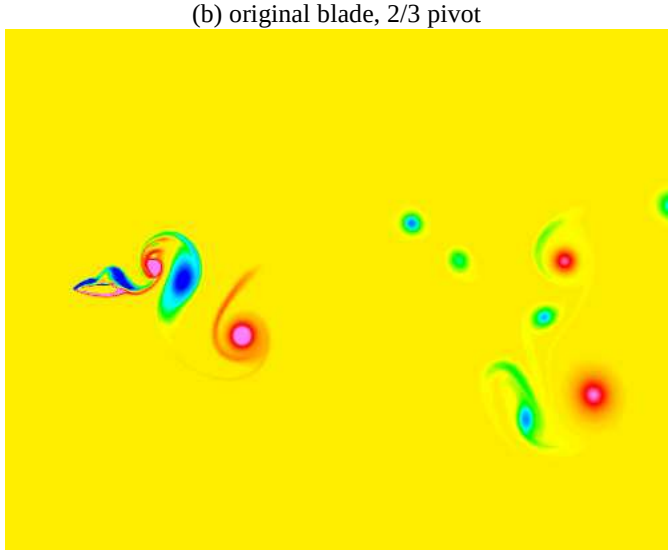

(c) thickest blade, 1/3 pivot

Figure 3, vorticity contours at blade position after 1/2 rotation

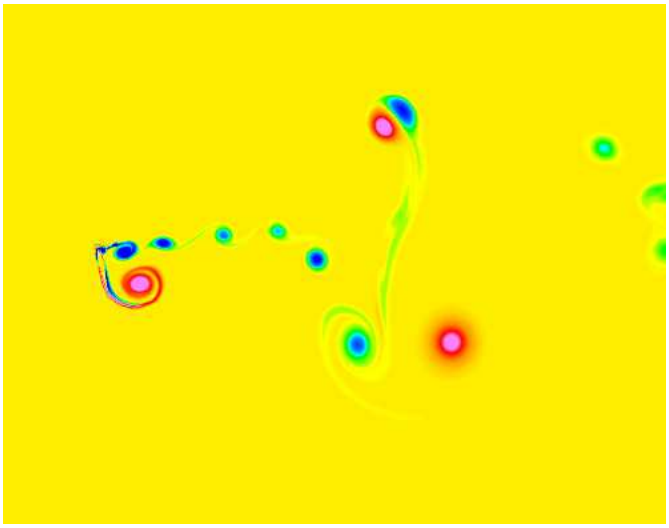

(a) original blade, 1/3 pivot

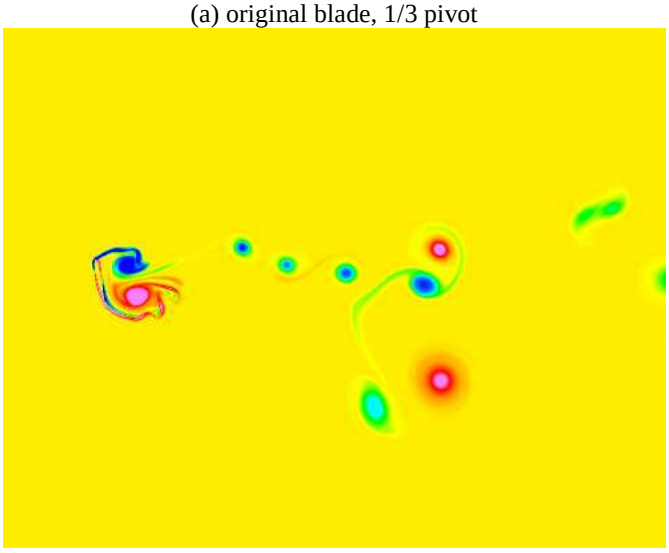

(b) original blade, 2/3 pivot

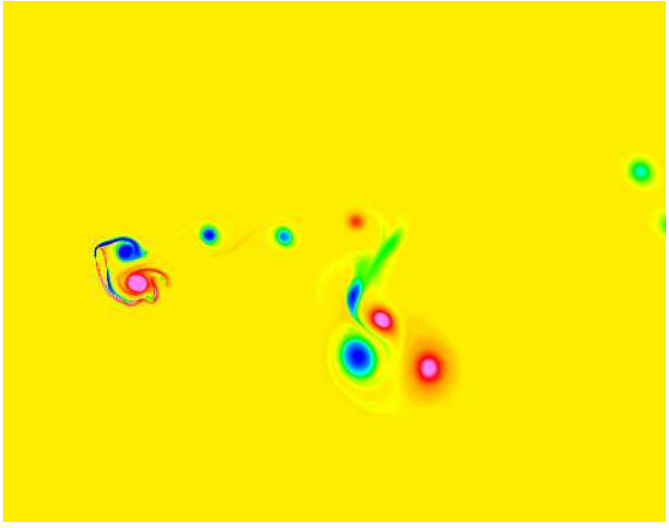

(c) thickest blade, 1/3 pivot

Figure 4, vorticity contours at blade position after 3/4 rotation

Figure 1 shows the z-directional (perpendicular to the plane) vorticity contours at the initial position, which is parallel to the flow, comparing them to different cases. At the initial position, the pivot location affects the vortex shedding pattern in the wake of the blade, while blade thickness has a relatively smaller effect on vortex shedding. The similar observations can be found in Figure 3 when the blade rotates half of the cycle again parallel to the flow with the trailing edge in the front. When the blade rotates at the vertical positions, the vortex shedding patterns among the three cases are different. It needs to be noted that although the positions in Figure 2 and 4 are symmetric, the vortex structures are different because of the counter-clockwise rotation of the blade while the free stream flow from left to right. In these two vertical positions, small and high frequency vortices were always generated from the tip on the top, which in Figure 2 is the trailing edge while it is the leading edge in Figure 4. The reason is these tips moved towards the free stream flow. The vortices generated on the other tip are larger and low frequency because the motion is the same at the flow direction. In the two parallel positions, large and low frequency vortices were generated.

Figure 5-8 are the comparisons of C_p distributions on the surface of the blade, at the same four blade rotation positions as in Figure 1-4. For all these figures, 0 to 3.14 radiant on x axis represents the same top surface of the blade as on the initial position, while 3.14 to 6.28 represents the same bottom surface of the blade. 0 represents the leading edge and 3.14 is the trailing edge.

One of the optimization criteria of the present turbine blade is the generation of the largest pushing force (drag force) for the turbine at one of the vertical positions (1/4 rotation) and the smallest pushing force when it is parallel to the flow and at the second vertical position (3/4 rotation). Figure 6 and 8 show the pressure coefficient at two vertical positions. In Figure 6, the top surface faces the flow while in Figure 8 the bottom surface faces the flow. From Figure 6, the original blade pivot is at 1/3 of the chord length and the thickest blade at the same pivot have the largest C_p on the top surface, but also largest on the bottom surface, and the original blade performs better than the thickest blade. The other three cases are about the same, and demonstrated that the C_p on the top and bottom surfaces are both lower than the C_p of original blade pivot at 1/3 chord length, and resulted in a similar pushing force. So the thickest blade performs the worst in Figure 6. At another vertical position, shown in Figure 8, the original blade pivot at 1/2 chord length shows the worst performance when compared to the others. The top surface has a much smaller C_p while the bottom surface (facing the flow) has one of the largest C_p. This results in a large pushing force which should be avoided.

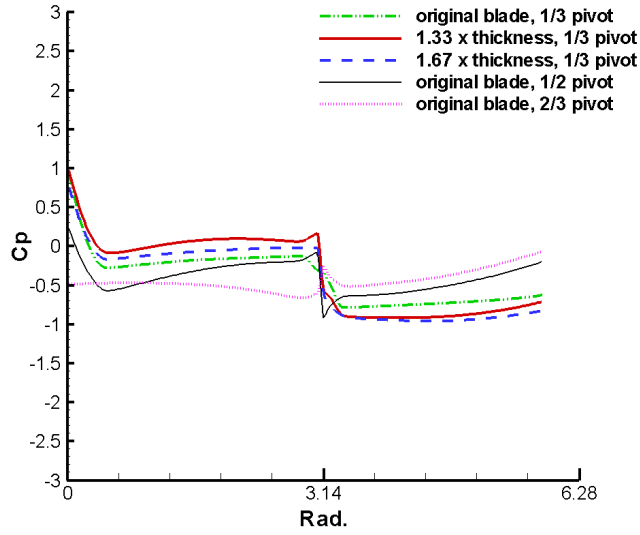

Figure 5, surface C_p comparison at initial position

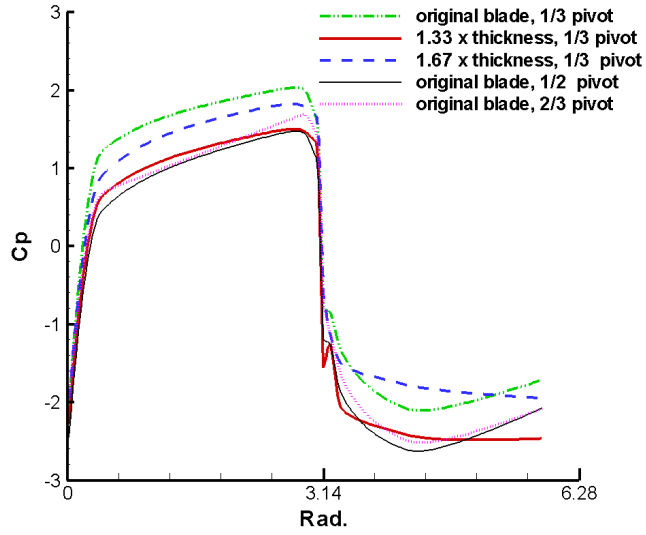

Figure 6, surface C_p comparison at position after 1/4 rotation

For the two parallel positions, Figure 5 is the initial position and Figure 7 is the position after the blade rotates 1/2 cycle. In Figure 5, among different thickness, the thinner the blade is, the smaller the pushing force (drag) is thus the better performance. When changing the pivot location, the shape of the curve changes, especially for pivot at 2/3 of the chord length which has negative C_p on most of the surface. Therefore, 2/3 pivot position with the thin blade performed the best in Figure 5. In Figure 7, the original thin blade at 1/3 pivot shows different distribution than the other cases, but the overall drag is small. Among other four cases, the thickest blade has the smallest C_p on most of its surface.

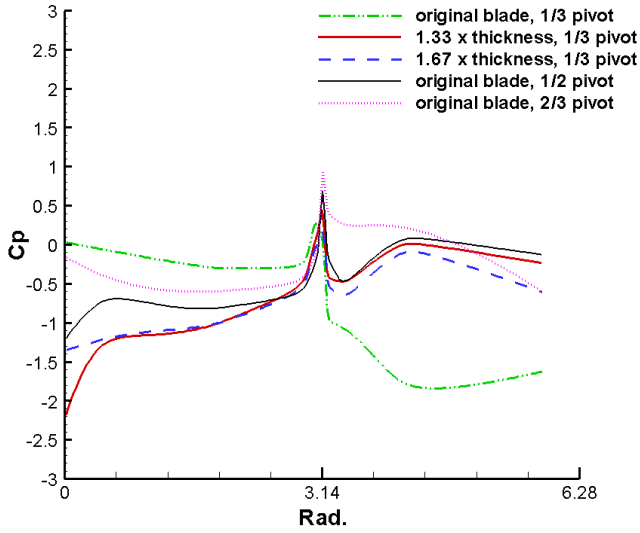

Figure 7, surface C_p comparison at position after 1/2 rotation

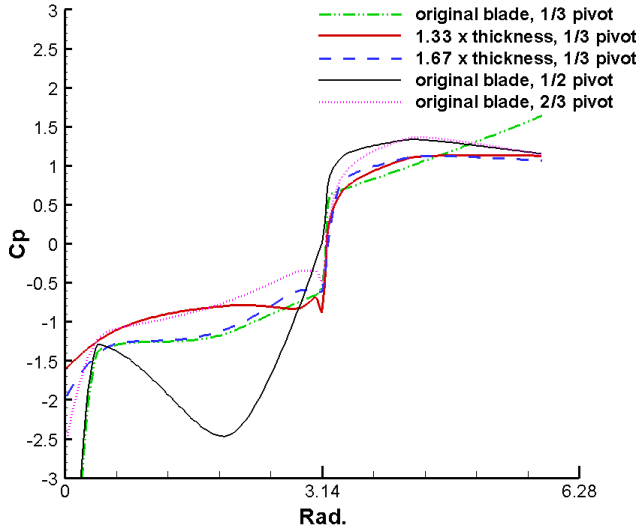

Figure 8, surface C_p comparison at position after 3/4 rotation

Figure 5-8 compared surface pressure coefficient among all the cases. The overall pressure drag at different blade positions dictates the performance of the turbine. The drag at the initial position is a negative effect in the actual turbine design, thus needs to be minimized. It is very small and obviously thinner blades are better choice, shown in Figure 5. At position after 1/2 rotation, the pressure drag is a positive effect to the turbine performance, because it is the major driving force to rotate the turbine. Figure 9 shows the overall pressure drag comparison at the moment. It is clear that, the

original blade at 1/3 pivot produced greatest drag. This means that the thin blade is also good for force generation of the turbine. When the blade thickness increases to 1.67 times, the turbine force generation significantly decreases. However, it needs to be mentioned that, thin blade is relatively hard to be installed on the turbine, and might not have enough strength. From Figure 9, the 1/3 pivot position is also better than the other two positions at this rotation position.

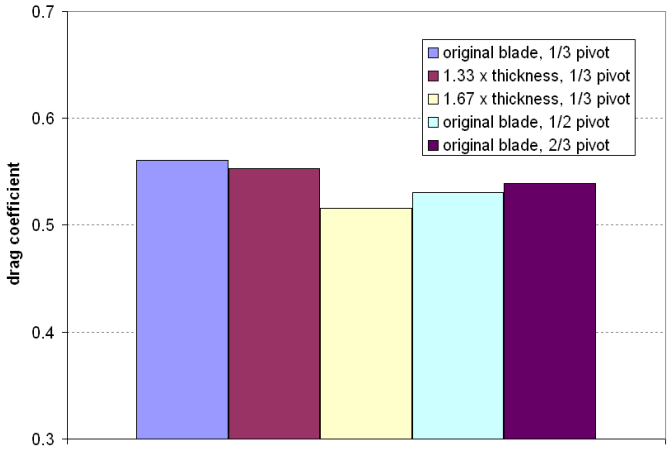

Figure 9, drag coefficient comparison at position after 1/2 rotation

CONCLUSIONS

Direct numerical simulations of flow over a rotating turbine blade were performed using the immersed-boundary method. The purpose was to investigate the flow and force characteristics to assist the turbine optimizations. Cases with different design parameters, including the blade thickness and pivot locations, were simulated. The complex vortex structures downstream of the blade were revealed. Small and high frequency vortices are generated from the tip moving towards the flow, while larger and low frequency vortices are generated at tips moving in other directions. The surface pressure coefficient at different rotating positions were plotted and analyzed. The overall drag coefficient was studied at the critical position for force generation. The results could assist with the design optimization. Overall, the thickest blade and pivot at 1/2 chord length should be avoided. The thin blade performs better than the thicker blades, and pivot at 2/3 shows the best performances at the initial position while pivot at 1/3 shows good performance at most of the positions.

ACKNOWLEDGMENTS

The financial support was provided by Gulfstream Technologies through McNeese State University.

REFERENCES

1. Zhang N., Zheng, Z.C., An Improved Direct-Forcing Immersed-Boundary Method for Finite Difference Applications, Journal of Computational Physics, Vol. 221, pp. 250-268, 2007
2. Triantafyllou, M.S., Techet, A.H., Hover, F.S., Review of experimental work in biomimetic foils. *IEEE Journal of Oceanic Engineering*, Vol. 29, pp. 585-594, 2004
3. Jones, K.D., Dohring, C.M., Platzer, M.F., Experimental and computational investigation of the Knoller-Berz effect. *AIAA J.*, Vol. 36, pp. 1240-1246, 1998
4. Koochesfahani, M., Vortical patterns in the wake of an oscillating foil. *AIAA J.*, 27, 1200-1205, 1989
5. Scherer, J.O., Experimental and theoretical investigation of large amplitude oscillating foil propulsion system. *U.S. Army Engineering Research and Development Laboratories*, 1968
6. Anderson, J.M., Streitlien, K., Barrett, D.S., Triantafyllou M.S., Oscillating foils of high propulsive efficiency. *J. Fluid Mech.*, Vol. 360, pp. 41-72, 1998
7. Read D.A., Hover, F.S., Triantafyllou, M.S., Forces on oscillating foils for propulsion and maneuvering. *Journal of Fluids and Structures*, Vol. 17, pp. 163-183, 2002
8. Webb, C., Dong, H., Michael, O., Effects of unequal pitch and plunge airfoil motion frequency on aerodynamic response. *46th AIAA Aerospace Sciences Meeting and Exhibit*, Jan. 7-10, 2008, Reno, Nevada, 2008
9. Lu, X.Y., Yang, J.M., Yin, X.Z., Propulsive performance and vortex shedding of a foil in flapping flight. *Acta Mechanica*, Vol. 165, pp. 189-206, 2003
10. Dong, H., Mittal, R., Najjar, F.M., Wake topology and hydrodynamics performance of low-aspect-ratio flapping foils. *J. Fluid Mech.*, vol. 566, pp. 309-343, 2006
11. Shen, W.Z., Sorensen J.N., Quasi-3D Navier-Stokes Model for a Rotating Airfoil, Journal of Computational Physics, Vol. 150, pp. 518-548, 1999
12. Goldstein, D., Handler, R., Sirovich, L., Modeling a no-slip flow boundary with an external force field. *J. Comp. Phys.*, Vol. 105, pp. 354-366, 1993
13. Saiki, E.M., Biringen, S., Numerical simulation of a cylinder in uniform flow: application of a virtual boundary method. *J. Comp. Phys.*, Vol. 123, pp. 450-465, 1996
14. Mohd-Yusof, J., Interaction of massive particles with turbulence. *Ph.D. Dissertation, Dept. of Mechanical and Aerospace Engineering, Cornell University*, 1996
15. Fadlun, E.A., Verzicco, R., Orlandi, P., Mohd-Yusof, J., Combined immersed-boundary finite-difference methods for three dimensional complex flow simulations. *J. Comp. Phys.*, Vol. 161, pp. 35-60, 2000
16. Ravoux, J.F., Nadim, A., Haj-Hariri, H., An embedding method for bluff body flows: interactions of two side-by-side cylinder wakes. *Theoret. Comput. Fluid Dyn.*, Vol. 16, pp. 433-466, 2003
17. Tseng Y.H., Ferziger, J.H., A ghost-cell immersed boundary method for flow in complex geometry. *J. Comp. Phys.*, Vol. 192, pp. 593-623, 2003
18. Mittal, R. and Iaccarino, G., Immersed boundary methods. *Annu. Rev. Fluid Mech.*, Vol. 37, pp. 239-261, 2005
19. Zheng, Z.C., Zhang, N., Frequency effects on lift and drag for flow past an oscillating cylinder. *Journal of Fluids and Structures*, Vol. 24, pp. 382-399, 2008
20. Zheng, Z. C., Zhang, N., Wei, Z., Low-Reynolds Number Simulation for Flow over a Flapping Wing: Comparisons to

Measurement Data, *Proc., 39th AIAA Fluid Dynamics Conference, June 22-25, San Antonio, TX*, 2009
21. Zhang, N., Zheng, Z.C., Flow/pressure characteristics for flow over two tandem swimming fish. *Computer & Fluids*, Vol. 38, pp. 1059-1064, 2009